SEECCM III
3rd South-East European Conference on Computational Mechanics-
an ECCOMAS and IACM Special Interest Conference
M. Papadrakakis, M. Kojic, I. Tuncer (eds.)
Kos Island, Greece, 12–14 June 2013

AN UNLOCKED IMPLICIT G^1 CONTINUITY MULTI PATCH B-SPLINE INTERPOLATION FOR THE ANALYSIS OF 3D KIRCHHOFF-LOVE ROD ELEMENTS

L. Greco[1], **M. Cuomo**[1], **N. Impollonia**[1]

[1]Dipartimento di Ingegneria Civile ed Ambientale (DICA)
Viale A. Doria 6, 95100 Catania, Italy
e-mail: mcuomo@dica.unict.it, leopoldo.greco@virgilio.it

Keywords: Isogeometric analysis, Kirchhoff-Love rod, G^1 multi patch analysis, geometric continuity, locking, assumed strain formulation

Abstract. *We present a multi patch assumed strain formulation (with implicit G^1-continuity at the ends of the element) for 3D space Kirchhoff-Love rod; rotations are introduced at the ends of the element as degree of freedom similarly to the Hermitian interpolation for Euler Bernoulli beam problem. In this way the G^1 continuity is ensured. Due to the general curved geometry a strong coupling appears in the membrane-flexural-torsion (m-f-t) problem, so that a pure displacement formulation leads in general to a locked element (membrane, flexural and torsion locking phenomena can occur). The multi patch approach presented, based on G^1 continuity (low degree of continuity), does not present locking in contrast to the B-Spline (high degree of continuity) element, in a pure displacement approach. However, both the approaches present spurious mode in the deformations, i.e. in the stress resultants. In order to avoid this pathology we adopt a standard assumed strain formulation (or B-bar) approach, projecting the tangent strain measures onto lower degree spaces, (by means of standard L^2 projections). In particular, considering a polynomial degree interpolation (p) for the displacements, the membrane and torsional strain measures are projected on a (p-1) space, while the two flexural strain measures are projected on a (p-2) space. In this way a very easy definition of the B-bar operators is attained, since the integrations are performed numerically. The strategy is very appealing for the design of free-locking general curve rod elements, and it provides very accurate results for different polynomial degrees as it is shown by means of presented example.*

1 INTRODUCTION

Displacement based formulations for structural model are known to suffer for locking phenomenon. In the case of general space curved K.L. rods a strong coupling appears in the membrane-flexural-torsion (m-f-t) problem, so that many source of locking affect the solution. In recent works [6, 7] Armero et al. have developed a new C^1 finite element for 3D Kirchhoff-Love rod adopting an assumed strain formulation, based on mixed (Hermitian and Lagrangian) interpolation, for overcoming the spurious strain modes. In [9] Elguedj et al., on the basis of [8], present a comparison between discrete strain gap (DSG) approach, as proposed in [5] by means of a collocation of the strain gaps, and the classical B-bar formulation for overcoming the locking in isogeometric analysis. They show that for both membrane and shear locking, the ASM approach is more accurate with respect to DSG. Locking in flexural an torsional dominated problems for curve elements is investigated in [10]. In [4] Beirao et al. present a collocation isogeometric approach to avoid the shear locking in beam. In this paper a multi-patch isogeometric formulation for K.L. rods is investigated, with respect to its ability to avoid locking.
In [3] a multi-patch isogeometric analysis of space rod by means of Lagrange's multipliers was presented. Multi-patch approaches with implicit G^1 continuity have been introduced in [2], in which it's proposed an element that consists in a generalization of standard cubic Hermite interpolation. It has been obtained performing a transformation on the displacement coordinate space, as illustrated in figure 1 for open Bspline generated by means of a knot vector with and without internal knots. The torsional angle ϕ is interpolated by means of a standard C^0 Bspline functions. In order to avoid locking an L^2 projection of the strains is considered, particularly, considering a p-degree interpolation for the degree of freedom $(\boldsymbol{u}, \phi)$ the function spaces for the axial, flexural and torsional strain measures are scaled, respectively, to $p-1$, $p-2$ and $p-1$ degree interpolations. In general, an isogeometric L^2 B-bar approach generates a full stiffness matrix, since the assumed strain interpolating bases are not-null everywhere. Contrarily to the high-continuity isogeometric B-bar formulation presented in [9], the multi patch G^1 continuous formulation presented in this paper allows to strongly reduces the band-width in the stiffness matrix.

2 THE INTERPOLATION

The multi patch isogeometric interpolation of non polar rods used in this paper has been introduced in [2]. It consists in a generalization of the Hermite interpolation to general open Bspline interpolations. The displacement degree of freedom of the the second and second last control points are re-parametrized introducing the end rotations as degree of freedom. Since the torsion angle ϕ is C^0 continuous, a G^1 constraints is ensured. The stiffness matrix is, then, easily assembled.

2.1 The G^1 interpolation of the centroid curve

At the ends of an open B-spline the tangent vector has the same direction defined by the two couple of end points. Let $\boldsymbol{P}_0(\lambda)$, with $\lambda \in [0,1]$, be the Lagrangian centroid curve. We adopt for the representation of this curve an open B-Spline description given by

$$\boldsymbol{P}_0(\lambda) = \Sigma_{i=1}^{n} b_i^p(\lambda)\mathbf{P}_{0,i} \tag{1}$$

where p is the degree and $n = p+1$ is the number of control points, $b_i^p(\lambda)$ is the i-th function and $\mathbf{P}_{0,i}$ is the generic control point. Let $\boldsymbol{p}(\lambda)$, with $\lambda \in [0,1]$, be the generic current centroid

curve,

$$\boldsymbol{p}(\lambda) = \Sigma_{i=1}^{n} b_i^p(\lambda)\mathbf{P}_i \tag{2}$$

A coordinate transformation is performed mapping the second, $\mathbf{P}_2$, and the second-last, $\mathbf{P}_{n-1}$, control points by means of the spatial rotations and the deformation of the end control segments directors $\tilde{\boldsymbol{t}}_{0,1}$ and $\tilde{\boldsymbol{t}}_{0,2}$ as follows

$$\mathbf{P}_2 = \mathbf{P}_1 + \rho_1 \tilde{\boldsymbol{R}}_1 \tilde{\boldsymbol{t}}_{0,1}, \quad \mathbf{P}_{n-1} = \mathbf{P}_n + \rho_2 \tilde{\boldsymbol{R}}_2 \tilde{\boldsymbol{t}}_{0,2}, \tag{3}$$

where the initial non unit directors are defined by the difference of the control points

$$\tilde{\boldsymbol{t}}_{0,1} = \mathbf{P}_{0,2} - \mathbf{P}_{0,1}, \quad \tilde{\boldsymbol{t}}_{0,2} = \mathbf{P}_{0,n-1} - \mathbf{P}_{0,n}, \tag{4}$$

in this way, from equation 3 the current non unit directors become

$$\tilde{\boldsymbol{t}}_1 = \mathbf{P}_2 - \mathbf{P}_1 = \rho_1 \tilde{\boldsymbol{R}}_1 \tilde{\boldsymbol{t}}_{0,1}, \quad \tilde{\boldsymbol{t}}_2 = \mathbf{P}_{n-1} - \mathbf{P}_n = \rho_2 \tilde{\boldsymbol{R}}_2 \tilde{\boldsymbol{t}}_{0,2}, \tag{5}$$

where $\tilde{\boldsymbol{R}}_1$ and $\tilde{\boldsymbol{R}}_2$ are the spatial rotations operators, and the scalars ρ_1 and ρ_2 are the relative change in the lengths of these vectors, given by

$$\rho_1 = \frac{\|\mathbf{P}_2 - \mathbf{P}_1\|}{\|\mathbf{P}_{0,2} - \mathbf{P}_{0,1}\|} = \frac{\|\tilde{\boldsymbol{t}}_1\|}{\|\tilde{\boldsymbol{t}}_{0,1}\|}, \quad \rho_2 = \frac{\|\mathbf{P}_{n-1} - \mathbf{P}_n\|}{\|\mathbf{P}_{0,n-1} - \mathbf{P}_{0,n}\|} = \frac{\|\tilde{\boldsymbol{t}}_2\|}{\|\tilde{\boldsymbol{t}}_{0,2}\|}. \tag{6}$$

The generic configuration of the centroid curve is given by

$$\begin{aligned}
\boldsymbol{p}(\lambda) =& b_1^p(\lambda)\mathbf{P}_1 + \\
&+ b_2^p(\lambda)\left(\mathbf{P}_1 + \rho_1 \tilde{\boldsymbol{R}}_1 \tilde{\boldsymbol{t}}_{0,1}\right) + \\
&+ b_3^p(\lambda)\mathbf{P}_3 + \ldots + b_{n-2}^p(\lambda)\mathbf{P}_{n-2} + \\
&+ b_{n-1}^p(\lambda)\left(\mathbf{P}_n + \rho_2 \tilde{\boldsymbol{R}}_2 \tilde{\boldsymbol{t}}_{0,2}\right) + \\
&+ b_n^p(\lambda)\mathbf{P}_n.
\end{aligned} \tag{7}$$

Observing that $\tilde{\boldsymbol{R}}_1^T \tilde{\boldsymbol{t}}_1 = \tilde{\boldsymbol{t}}_{0,1}$ and $\tilde{\boldsymbol{R}}_2^T \tilde{\boldsymbol{t}}_2 = \tilde{\boldsymbol{t}}_{0,2}$ and that $\dot{\tilde{\boldsymbol{R}}}_1 \tilde{\boldsymbol{R}}_1^T = \tilde{\boldsymbol{\omega}}_1 \times (\bullet)$ and $\dot{\tilde{\boldsymbol{R}}}_2 \tilde{\boldsymbol{R}}_2^T = \tilde{\boldsymbol{\omega}}_2 \times (\bullet)$ the velocity of the centroid curve mapped as in equation 7 is given by

$$\begin{aligned}
\dot{\boldsymbol{p}}(\lambda) =& \left(b_1^p(\lambda) + b_2^p(\lambda)\right)\dot{\mathbf{P}}_1 + \\
&+ b_2^p(\lambda)\left(-\rho_1\, \tilde{\boldsymbol{t}}_1 \times \tilde{\boldsymbol{\omega}}_1 + \dot{\rho}_1\, \tilde{\boldsymbol{t}}_1\right) \\
&+ b_3^p(\lambda)\dot{\mathbf{P}}_3 + \ldots + b_{n-2}^p(\lambda)\dot{\mathbf{P}}_{n-2} + \\
&+ b_{n-1}^p(\lambda)\left(-\rho_2\, \tilde{\boldsymbol{t}}_2 \times \tilde{\boldsymbol{\omega}}_2 + \dot{\rho}_2\, \tilde{\boldsymbol{t}}_2\right) \\
&+ \left(b_n^p(\lambda) + b_{n-1}^p\right)\dot{\mathbf{P}}_n.
\end{aligned} \tag{8}$$

2.2 The C^0 interpolation of the torsional angle

The tangent increment of the torsional angle is given by

$$\dot{\phi}(\lambda) = \Sigma_{i=1}^{n} b_i^p(\lambda)\dot{\phi}_i \tag{9}$$

but the first and the last term must be represented in terms of the end rotations, observing that $\hat{\boldsymbol{t}}\big|_0 = \hat{\tilde{\boldsymbol{t}}}_1$ and $\hat{\boldsymbol{t}}\big|_1 = -\hat{\tilde{\boldsymbol{t}}}_2$ and that $\dot{\phi} = \tilde{\boldsymbol{\omega}} \cdot \hat{\boldsymbol{t}}$ the interpolation of the velocity of rotation around the centroid curve, is

$$\begin{aligned}\dot{\phi}(\lambda) =& b_1^p(\lambda)\, \tilde{\boldsymbol{\omega}}_1 \cdot \hat{\tilde{\boldsymbol{t}}}_1 + \\ &+ b_1^p(\lambda)\dot{\phi}_2 ... + b_{n-1}^p(\lambda)\dot{\phi}_{n-1} \\ &+ b_n^p(\lambda)\, \tilde{\boldsymbol{\omega}}_2 \cdot (-\hat{\tilde{\boldsymbol{t}}}_2).\end{aligned} \tag{10}$$

Considering, for each control point, the vector of the increments of the degrees of the freedom $\dot{\boldsymbol{q}}$ defined as

$$\dot{\boldsymbol{q}}^T = \{\dot{\mathbf{P}}_1, \tilde{\boldsymbol{\omega}}_1, \dot{\rho}_1, \dot{\phi}_2; \dot{\mathbf{P}}_3, \dot{\phi}_3, ..., \dot{\mathbf{P}}_{n-2}, \dot{\phi}_{n-2}; \dot{\phi}_{n-1}, \dot{\rho}_2, \dot{\mathbf{P}}_n, \tilde{\boldsymbol{\omega}}_2\} \tag{11}$$

the velocity of the centroid curve, $\boldsymbol{p}$, and of the torsional angle, ϕ, are given respectively by

$$\dot{\boldsymbol{p}}(\lambda)^{3,1} = \mathbb{B}_c^p(\lambda)^{3,4n}\, \dot{\boldsymbol{q}}^{4n,1} \tag{12}$$

and

$$\dot{\phi}(\lambda) = \mathbb{B}_\phi^p(\lambda)^{1,4n}\, \dot{\boldsymbol{q}}^{4n,1}, \tag{13}$$

where the operators $\mathbb{B}_c^p(\lambda)$ and $\mathbb{B}_\phi^p(\lambda)$ are defined as

$$\begin{aligned}\mathbb{B}_c^p(\lambda) = \{&(b_1^p + b_2^p)\, \boldsymbol{I}^{\,3,3},\ -b_2^p\, (\tilde{\boldsymbol{t}}_1 \times (\bullet))^{\,3,3},\ b_2^p\, (\tilde{\boldsymbol{t}}_1)^{\,3,1},\ \mathbf{0}^{\,3,1}, \\ &b_3^p\, \boldsymbol{I}^{\,3,3}, \mathbf{0}^{\,3,1}, ...,\ b^{n-2} \boldsymbol{I}^{\,3,3},\ \mathbf{0}^{\,3,1}, \\ &\mathbf{0}^{\,3,1},\ b_{n-1}^p (\tilde{\boldsymbol{t}}_2)^{\,3,1},\ (b_{n-1}^p + b_n^p) \boldsymbol{I}^{\,3,3},\ -b_{n-1}^p (\tilde{\boldsymbol{t}}_2 \times (\bullet))^{\,3,3}\},\end{aligned} \tag{14}$$

and

$$\begin{aligned}\mathbb{B}_\phi^p(\lambda) = \{&(\mathbf{0}^T)^{\,1,3},\ b_1^p\, (\tilde{\boldsymbol{t}}_1^T)^{\,1,3},\ 0,\ b_2^p, \\ &(\mathbf{0}^T)^{\,1,3},\ b_3^p, ...,\ (\mathbf{0}^T)^{\,1,3},\ b_{n-2}^p, \\ &b_{n-1}^p,\ 0,\ (\mathbf{0}^T)^{\,1,3},\ b_n^p\, (\tilde{\boldsymbol{t}}_2^T)^{\,1,3}\}.\end{aligned} \tag{15}$$

where $\boldsymbol{I}$ is the identity operator, $\mathbf{0}^T = \{0, 0, 0\}$ and

$$-\tilde{\boldsymbol{t}}_j \times (\bullet) = \begin{pmatrix} 0 & +\tilde{\boldsymbol{t}}_j \cdot \boldsymbol{E}_z & -\tilde{\boldsymbol{t}}_j \cdot \boldsymbol{E}_y \\ -\tilde{\boldsymbol{t}}_j \cdot \boldsymbol{E}_z & 0 & +\tilde{\boldsymbol{t}}_j \cdot \boldsymbol{E}_x \\ +\tilde{\boldsymbol{t}}_j \cdot \boldsymbol{E}_y & -\tilde{\boldsymbol{t}}_j \cdot \boldsymbol{E}_x & 0 \end{pmatrix}, \quad \tilde{\boldsymbol{t}}_j = \begin{pmatrix} \tilde{\boldsymbol{t}}_j \cdot \boldsymbol{E}_x \\ \tilde{\boldsymbol{t}}_j \cdot \boldsymbol{E}_y \\ \tilde{\boldsymbol{t}}_j \cdot \boldsymbol{E}_z \end{pmatrix}, \quad j = 1, 2. \tag{16}$$

Figures 1(a) and 1(b) are related to Bernstein's polynomials of degree 3 and it is clear that the transformation proposed yields to the Hermite shape functions. Figures 1(c) and 1(d) are related to Bernstein's polynomials of degree 4 and corresponding transformed G^1-functions; Figures 1(e) and 1(f) are related to a B-Spline of degree 3 with internal knots and corresponding transformed G^1-B-Spline.

2.3 Strain measures

The velocity of the deformations have been evaluated [1, 2] and are represented by means of the compatibility operators, $\boldsymbol{B}_{(\bullet)}$, as follows:

$$\begin{aligned}\varepsilon(\boldsymbol{q}_0, \dot{\boldsymbol{q}}) = \boldsymbol{B}_\varepsilon^T(\boldsymbol{q}_0)\dot{\boldsymbol{q}}, \quad \chi_n(\boldsymbol{q}_0, \dot{\boldsymbol{q}}) = \boldsymbol{B}_{\chi_n}^T(\boldsymbol{q}_0)\dot{\boldsymbol{q}} \\ \chi_\nu(\boldsymbol{q}_0, \dot{\boldsymbol{q}}) = \boldsymbol{B}_{\chi_\nu}^T(\boldsymbol{q}_0)\dot{\boldsymbol{q}}, \quad \gamma(\boldsymbol{q}_0, \dot{\boldsymbol{q}}) = \boldsymbol{B}_\gamma^T(\boldsymbol{q}_0)\dot{\boldsymbol{q}}.\end{aligned} \tag{17}$$

3 THE ASSUMED STRAIN FORMULATION

The assumed strain method (ASM), proposed in [6, 8, 9] consists in a L^2-projection of the strain measures, by means of the weak definition of the compatibility equation. Let b_i^p be the generic i-th function of degree p, that interpolates the displacement field $\boldsymbol{q} = (\boldsymbol{u}, \phi)$. The axial, bending and twisting deformations are projected onto the spaces, respectively, b_ε^{p-1}, b_χ^{p-2} and b_γ^{p-1}, with lower polynomial and continuity degrees. A B-bar formulation for G^1 multi-patch interpolations with *BSpline* without internal knots is presented next. We remark that, the displacements functional space adopted is G^1 continuous as defined in the previous section, while the strain measures are projected onto standard open BSpline space with lower polynomial degree and lower parametric continuity.

3.1 The B-bar operators

For the Kirchhoff-Love rod the strain measures consistent with a (weak) compatibility conditions are given by modified $\bar{\boldsymbol{B}}$-operators

$$\bar{\varepsilon}(\dot{\boldsymbol{d}}) = \bar{\boldsymbol{B}}_\varepsilon^T \dot{\boldsymbol{d}}, \quad \bar{\chi_n}(\dot{\boldsymbol{d}}) = \bar{\boldsymbol{B}}_{\chi_n}^T \dot{\boldsymbol{d}}, \quad \bar{\chi_\nu}(\dot{\boldsymbol{d}}) = \bar{\boldsymbol{B}}_{\chi_\nu}^T \dot{\boldsymbol{d}}, \quad \bar{\gamma}(\dot{\boldsymbol{d}}) = \bar{\boldsymbol{B}}_\gamma^T \dot{\boldsymbol{d}}, \tag{18}$$

where these modified $\bar{\boldsymbol{B}}$-operators are given by

$$\bar{\boldsymbol{B}}_\varepsilon^T = (\boldsymbol{b}^{p-1})^T \bar{\boldsymbol{G}}^{-1} \int_L \left(\boldsymbol{b}^{p-1} \boldsymbol{B}_\varepsilon^T\right) dL, \quad \bar{\boldsymbol{B}}_\gamma^T = (\boldsymbol{b}^{p-1})^T \bar{\boldsymbol{G}}^{-1} \int_L \left(\boldsymbol{b}^{p-1} \boldsymbol{B}_\gamma^T\right) dL, \tag{19}$$

and

$$\bar{\boldsymbol{B}}_{\chi_n}^T = (\boldsymbol{b}^{p-2})^T \bar{\bar{\boldsymbol{G}}}^{-1} \int_L \left(\boldsymbol{b}^{p-2} \boldsymbol{B}_{\chi_n}^T\right) dL, \quad \bar{\boldsymbol{B}}_{\chi_\nu}^T = (\boldsymbol{b}^{p-2})^T \bar{\bar{\boldsymbol{G}}}^{-1} \int_L \left(\boldsymbol{b}^{p-2} \boldsymbol{B}_{\chi_\nu}^T\right) dL, \tag{20}$$

in which the $\bar{\boldsymbol{G}}$ and $\bar{\bar{\boldsymbol{G}}}$ are the corresponding *mass* matrices

$$\bar{\boldsymbol{G}} = \int_L \left(\boldsymbol{b}^{p-1} \otimes \boldsymbol{b}^{p-1}\right) dL, \quad \bar{\bar{\boldsymbol{G}}} = \int_L \left(\boldsymbol{b}^{p-2} \otimes \boldsymbol{b}^{p-2}\right) dL. \tag{21}$$

The stiffness operator is defined analogously to a pure displacement formulation. Numeric integration is performed at level of the element considering $p+1$ Gauss-Lobatto points.

4 NUMERICAL EXAMPLES

In this section three simple cases of curved rods are considered in which the case of membrane, flexural and both locking pathologies. The material parameters are $E = 2{*}10^8\,[kN/m^2]$, $\nu = 0.25$. The radius of the centroid is $R = 1\,[m]$ and the force at the end has intensity $\|f\| = 1\,[kN]$. In the first two numerical example $\hat{\boldsymbol{n}}(S) = \hat{\boldsymbol{e}}_z = \{0, 0, 1\}$ and $\hat{\boldsymbol{\nu}}(S) = \hat{\boldsymbol{t}} \times \hat{\boldsymbol{n}}(S)$ are considered while in the last example an initial torsion angle $\phi(S) = \frac{\pi S}{2}$ it is considered.

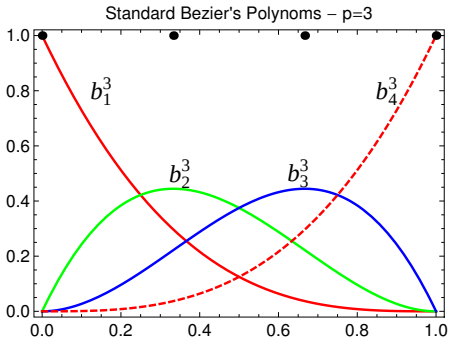

(a) C^0 Bernstein interpolation functions (polynomial degree p=3).

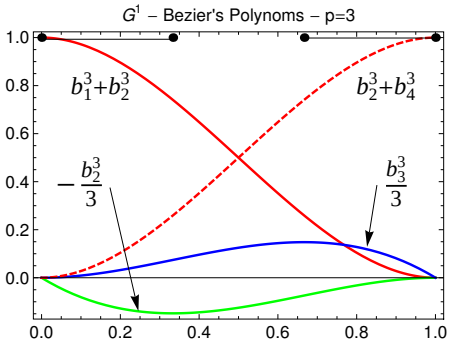

(b) G^1 Bernstein interpolation functions (Hermitian f. p=3).

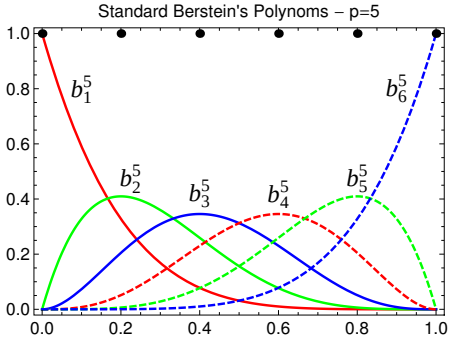

(c) C^0 Bernstein interpolation functions (polynomial degree p=5).

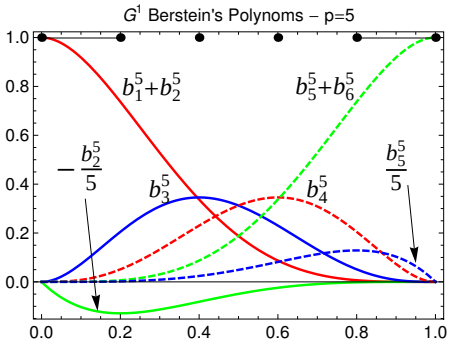

(d) G^1 Bernstein interpolation functions (polynomial degree p=5).

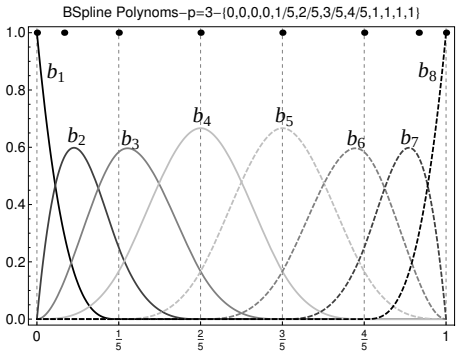

(e) Standard C^0 open BSpline interpolation (polynomial degree p=3).

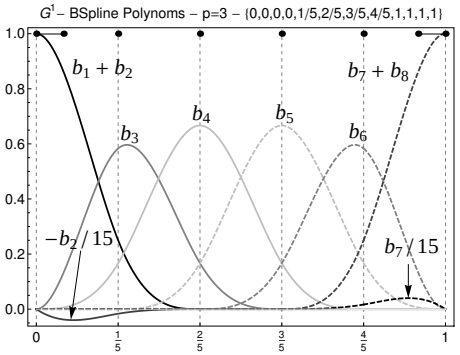

(f) G^1 open BSpline interpolation (polynomial degree p=3).

Figure 1: Transformation of shape function from standard C^0 open BSpline to G^1 open BSpline shape functions, (with or without internal knots).

4.1 Example 1: 2D Arch with a point force at the end

In this section it is considered a circular 2D arch with a point force at the end, see figure 2(a). Figures 2(b) and 2(c) show the comparison in the error in L^2 norm for the u_y displacement's component, (for two polynomials degrees $p = 3, 4$), between a pure displacement and B-bar approach, in the case of multi patch interpolation. The rate of the convergence is highlighted. Figures 2(d) and 2(e) show the L^2 error with the ratio R/h_ν for different discretizations, either

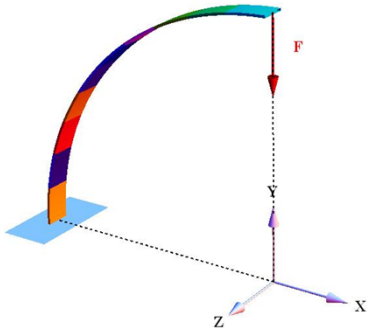

(a) Geometry

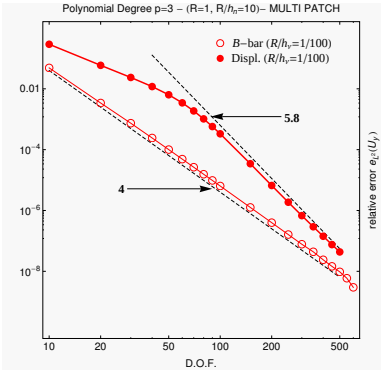

(b) u_y error in L^2 norm for p=3, (pure displ. vs. B-bar)

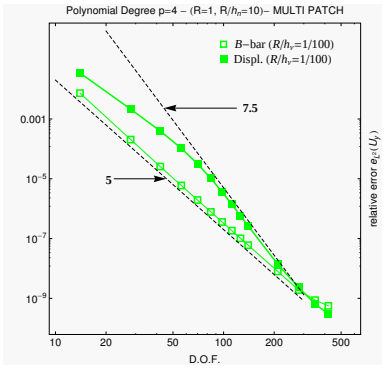

(c) u_y error in L^2 norm for p=4, (pure displ. vs. B-bar)

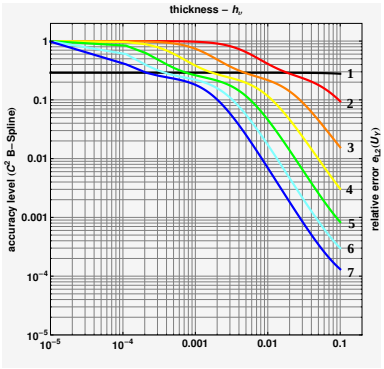

(d) High inter-element continuity BSpline (pure displ.)

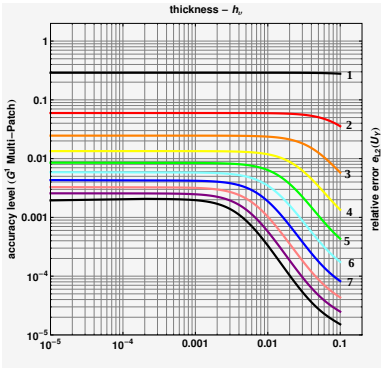

(e) Low inter element continuity G^1-multi-patch (pure displ.)

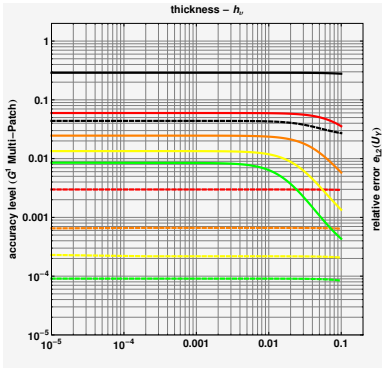

(f) G^1-multi-patch pure displ. vs. ASM (or B-bar dashed line).

Figure 2: Cantilever 2D arch with a shear at the end, (membrane locking).

for a BSpline and a multi patch approach; drastic membrane locking appears in the case of Bspline interpolation that disappears in the case of the multi patch approach. However spurious modes occurs on the axial stress that is reflected in a reduction of the accuracy in the solution, see Figure 2(e). Therefore a B-bar approach is necessary for an accurate definition of the strains in a multi patch approach. Figure 2(f) show the comparison between the accuracy level obtained with a pure displacement and a $\bar{B}$ formulation in the case of the multi-patch approach.

4.2 Example 2: 3D Arch with a point force at the end

In this section it is considered a circular 3D arch with a point force at the end, see figure 3(a). Figure 3(b) shows the comparison for the convergence's rate of the relative L^2 error norm for

the u_z solution, (for the polynomials degree $p = 3$ and ratio $R/h_\nu = 100$), between the pure displacement and the $\bar{B}$ formulation both the case of the G^1-multi-patch approach. Figure 4(d)

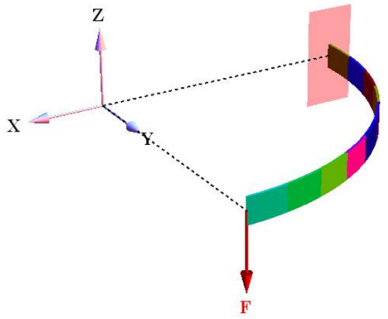

(a) Geometry

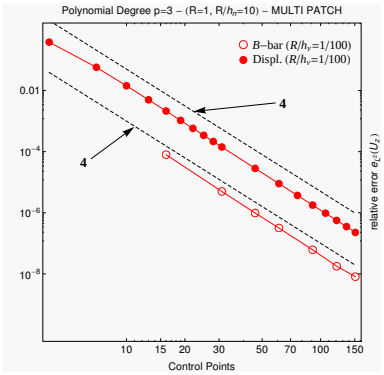

(b) u_z error in L^2 norm for p=3, (pure displ. vs. B-bar)

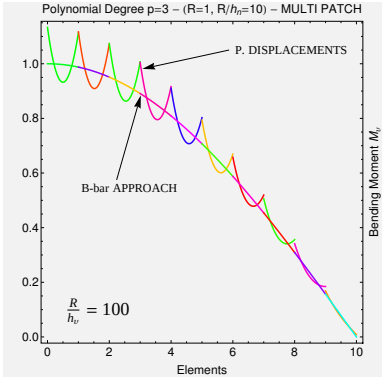

(c) Bending moment M_ν comparisons $\bar{B}$ vs P. Displacements

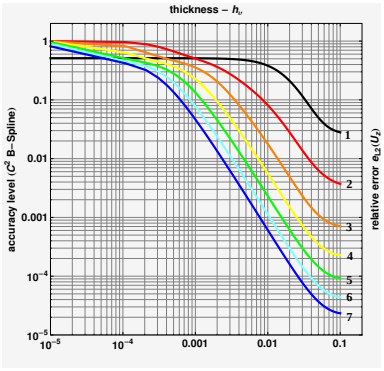

(d) High inter-element continuity BSpline (pure displ.)

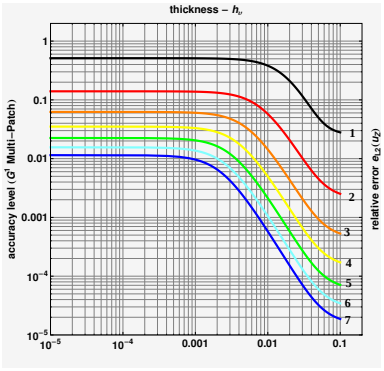

(e) Low inter element continuity G^1-multi-patch (pure displ.)

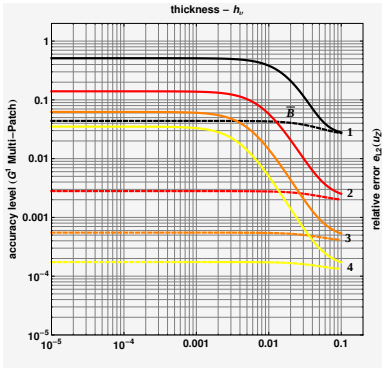

(f) G^1-multi-patch pure displ. vs. ASM (or B-bar dashed line).

Figure 3: Cantilever 3D arch with a shear at the end, (flexural locking).

and 4(e) show the error in L^2 norm as function of the ratio R/h_ν for different discretizations in the case of BSpline (high inter element continuity) and in the case of the G^1 multi-patch approach (low inter element continuity), for a pure displacement formulation. In the case of the BSpline interpolation flexural locking appears while in the case of the multi patch approach no locking appears. As previously observed oscillations can occur in the bending moment M_ν for a pure displacement approach so that a $\bar{B}$ formulation is necessary. For the multi patch approach only, figure 3(f) shows the comparison in the accuracy level obtained with a pure displacement and a $\bar{B}$ (dashed lines) formulation respectively.

4.3 Example 3: 3D pre-twisted arch with a point force at the end

In this section is considered a pre-twisted circular 3D arch with a shear at the end, see figure 4(a). Figure 4(b) shows the comparison for the convergence rate of the error in L^2 norm of the u_z displacement component, (for polynomial degrees $p = 3, 4$), for the G^1 multi-patch approach using the pure displacement and the $\bar{B}$ formulation. Figure 4(c) shows a real example of a pre-

twisted curve rod, i.e. a *Glulam* pre-twisted curve wood beam. Figure 4(d) and 4(e) show the

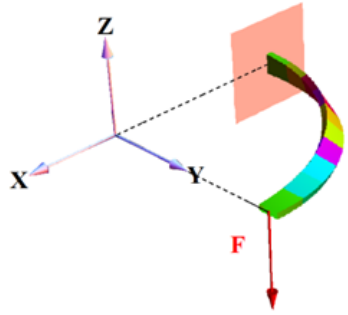

(a) Geometry

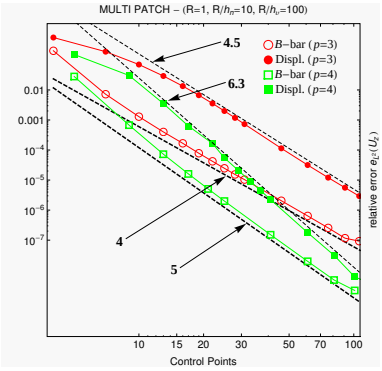

(b) u_z error in L^2 norm for p=3,4, (pure displ. vs. B-bar)

(c) Wood realization, bent and twisted curved *Glulam* beam.

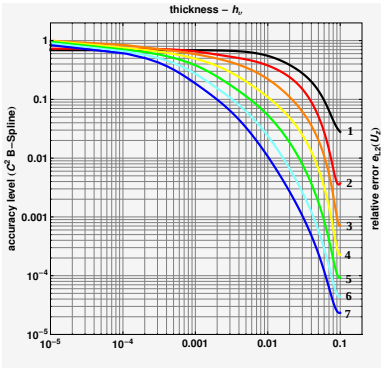

(d) High inter-element continuity BSpline (pure displ.)

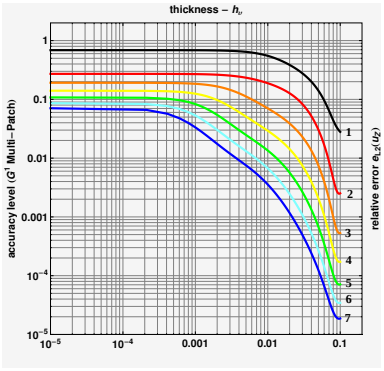

(e) Low inter element continuity G^1-multi-patch (pure displ.)

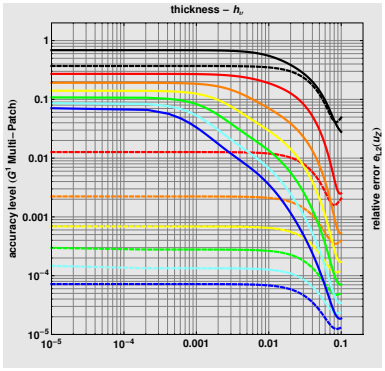

(f) G^1-multi-patch pure displ. vs. ASM (or B-bar dashed line).

Figure 4: Pre-twisted cantilever 3D arch with a shear at the end, (flexural locking).

trend of the L^2 error norm with respect to the ratio R/h_ν for different discretizations, in the case of BSpline (high-continuity) and G^1 multi-patch approaches; As opposite to the displacement formulations, no flexural locking appears in the multi patch approach but significative oscillations can occur in the bending deformations. A $\bar{B}$ approach solve this problem as shown figure 4(f) when a comparison in the accuracy level between pure displacement and $\bar{B}$ (dashed lines) for multi-patch approach are presented.

5 CONCLUSIONS

- The paper has presented a isogeometric generalization of the G^1-Hermitian interpolation for 3D space Kirchhoff-Love rods.
- The influence of the inter element continuity level on the locking phenomena for 3D Kirchhoff-Love space rods has been show, comparing the case of Bspline and G^1-multi patch approaches. The multi patch approach strongly reduce locking.

- A G^1-multi patch assumed strain formulation has been presented, (in which is obtained a banded stiffness matrix contrary to the case of BSpline interpolation); It reduces the oscillations in the stress resultants.

REFERENCES

[1] L. Greco, M. Cuomo, B-Spline interpolation of Kirchhoff-Love space rods. *Computer Methods in Applied Mechanics and Engineering*, http://dx.doi.org/10.1016/j.cma.2012.11.017, available online 5 December 2012.

[2] L. Greco, M. Cuomo, An implicit G^1 continuity B-Spline interpolation for the analysis of 3D-Space assembly of Kirchhhoff-Love rods. *submitted to CMAME, 2013*,

[3] L. Greco, Multi-patch isogeometric analysis of space rods. *YIC2012*, 24-27 April, Aveiro, Portugal.

[4] L. Beirao, C. Lovadina, A. Reali Avoiding shear locking for the Timoshenko beam problem vai isogeometric collocation methods. *Computer Methods in Applied Mechanics and Engineering*, **241-244**, 38–51, 2012.

[5] R. Echter, M. Bischoff Numerical efficiency, locking and unlocking of NURBS finite elements. *Computer Methods in Applied Mechanics and Engineering*, **199**, 374–382, 2010.

[6] F. Armero, J. Valverde, Invariant Hermitian Finite Elements for Thin Kirchhoff Love Rods. I: The linear Plane Case. *Computer Methods in Applied Mechanics and Engineering*, **213-216**, 458–485, 2012.

[7] F. Armero, J. Valverde, Invariant Hermitian Finite Elements for Thin Kirchhoff Love Rods. II: The Linear Three-Dimensional Case. *Computer Methods in Applied Mechanics and Engineering*, **213-216**, 427–457, 2012.

[8] T. Elguedj, Y. Bazilevs, V.M. Calo, T.J.R. Hughes, B-bar and F-bar Projection Methods for Nearly Incompresible Linear and Nonlinear Elasticity and Plasticity using Higher-order NURBS Elements. *Computer Methods in Applied Mechanics and Engineering*, **197**, 5257–5296, 2007.

[9] R. Bouclier, T. Elguedj, A. Comberscure, Locking free isogeometric formulation of curved thick beams. *Computer Methods in Applied Mechanics and Engineering*, **245-246**, 144–162, 2012.

[10] Md. Ishaquddin, P. Raveendranath, J.N. Reddy, Flexure and torsion locking phenomena in out-of-plane deformation of Timoshenko curved beam element. *Finite Elements in Analysis and Design*, **51**, 22–30, 2012.